J Ginseng Res 44 (2020) 823–832

Contents lists available at ScienceDirect

Journal of Ginseng Research

journal homepage: http://www.ginsengres.org

Research Article

# Bone remodeling effects of Korean Red Ginseng extracts for dental implant applications

Myong-Hun Kang [1], Sook-Jeong Lee [2,*], Min-Ho Lee [1,**]

[1] Department of Dental Biomaterials and Institute of Biodegradable Materials, Institute of Oral Bioscience and School of Dentistry (Plus BK21 Program), Jeonbuk National University, Jeonju, Jeollabuk-do, Republic of Korea
[2] Department of Bioactive Material Science, Jeonbuk National University, Jeonju, Jeollabuk-do, Republic of Korea

ARTICLE INFO

*Article history:*
Received 16 December 2019
Received in Revised form
9 May 2020
Accepted 15 May 2020
Available online 27 May 2020

*Keywords:*
Korean Red Ginseng extracts
Osseointegration
Osteogenesis
Titanium miniimplant
Titanium nanotubes

ABSTRACT

*Background:* The formation of a nanotube layer on a titanium nanotube (N-Ti) plate facilitates an active reaction between bone cells and the material surface via efficient delivery of the surface materials of the dental implant into the tissues. Studies have reported that Korean Red Ginseng extracts (KRGEs) are involved in a variety of pharmacological activities: we investigated whether implantation with a KRGE-loaded N-Ti miniimplant affects osteogenesis and osseointegration.
*Methods:* KRGE-loaded nanotubes were constructed by fabrication on pure Ti via anodization, and MC3T3-E1 cells were cultured on the N-Ti. N-Ti implants were subsequently placed on a rat's edentulous mandibular site. New bone formation and bone mineral density were measured to analyze osteogenesis and osseointegration.
*Results:* KRGE-loaded N-Ti significantly increased the proliferation and differentiation of MC3T3-E1 cells compared with cells on pure Ti without any KRGE loading. After 1–4 weeks, the periimplant tissue in the edentulous mandibular of the healed rat showed a remarkable increase in new bone formation and bone mineral density. In addition, high levels of the bone morphogenesis protein-2 and bone morphogenesis protein-7, besides collagen, were expressed in the periimplant tissues.
*Conclusion:* Our findings suggest that KRGE-induced osteogenesis and osseointegration around the miniimplant may facilitate the clinical application of dental implants.


## 1. Introduction

Dental materials are used to restore normal function in patients recovering from paralysis, disease, esthetic and linguistic problems, and injuries of the oral and maxillofacial system. A dental implant is an ideal choice for patients who have lost teeth due to periodontal disease or injury; the healing process after dental implantation requires approximately 3–6 months or longer depending on the condition. Dental materials are the closest in size and shape to the natural tooth root.

Osseointegration occurs during the healing period, when the bone tissues attach to the implant, forming a strong structural bond [1]; osseointegration is defined as the direct connection between an implant and bone, with no soft tissue interference. The concept of osseointegration was first introduced in dentistry in the early 1960s and was used to restore oral functions in elderly patients [2]. Osseointegration plays a key role in the success of an implant and its subsequent stability owing to its importance in the function of osteoblasts and connective tissues [3]. These methods show significant differences and characteristics depending on multiple factors, such as the interface between the implant and abutment, implant shape, and the implant and bone surfaces.

A recent study of the interaction between osteocytes and Ti nanotube (N-Ti) implants reported that the structure of nanotubes influences osteoblast adhesion, proliferation, and cell migration [4]. The N-Ti formed via anodization promotes osteoblast activity and interaction by increasing the contact area between the osteocytes and the implant. Furthermore, the selective release of biomolecules and drug delivery between the implant surface and bone are important for successful dental implantation [5,6].

* Corresponding author: Department of Bioactive Material Science, Jeonbuk National University, 567 Baekje-daero, Deokjin-gu, Jeonju, Jeollabuk-do,54896, Republic of Korea.
** Corresponding author: Department of Dental Biomaterials, Jeonbuk National University, 567 Baekje-daero, Deokjin-gu, Jeonju, Jeollabuk-do,54896, Republic of Korea.
*E-mail addresses:* sj@jbnu.ac.kr (S.-J. Lee), mh@jbnu.ac.kr (M.-H. Lee).

https://doi.org/10.1016/j.jgr.2020.05.003
p1226-8453 e2093-4947/$ – see front matter 

Recently, natural drugs have come under close investigation as they are significantly safer than synthetic drugs [7,8]. The search for novel pharmacotherapy derived from medicinal plants has significantly progressed. *Panax ginseng* (Korean ginseng) is commonly used for medical purposes. The main physiologically active substances in Red ginseng include saponins, essential oils, polyacetylene, phenols, glycosides, and peptides. Red ginseng also contains various vitamins, sugars, and minerals, which act as excellent antioxidants and antiaging agents. Among them, ginsenosides are the major components with respect to pharmacological effects [9]. Shibata et al [8] designated glycosides in ginseng as ginsenosides. The ginsenosides Rg2, Rg3, Rh1, and Rh2 are unique ingredients in ginseng, generated via thermal stimulation, and have been found effective in cancer prevention, cancer cell growth inhibition, blood pressure control, diabetes management, neuroprotection, reduction of inflammation and fatigue, and strengthening of immune responses [10–12]. In addition, the ginsenosides Rb1, Rg1, and Re have been found to be effective regulators of bone metabolism and influencers on osteoporotic bone loss, mesenchymal stem cell biology, and osteoclast differentiation [13–15].

For the successful dental implant, the morphogenic structure and material loaded onto the implant surface play a key role in ensuring the persistence and stability of the implant by increasing osseointegration between the bone and the implant. In this study, we examined whether Korean Red Ginseng extract (KRGE)–loaded N-Ti (GN-Ti) implants can be used as potential drug delivery systems and whether they affect postimplant osseointegration and osteogenesis.

## 2. Materials and methods

### 2.1. Preparation of pure Ti and fabrication of $TiO_2$ nanotubes on pure Ti plates

The specimens used in this study were prepared by cutting pure Ti (P-Ti) plates (Grade 2, Kobe Steel Ltd., Kobe, Japan). P-Ti foil of different sizes was polished using 400–1000 grit emery paper and subsequently washed with acetone and distilled water in an ultrasonic cleaner. $TiO_2$ nanotubes were fabricated using an anodization process, as described previously [16]. Anodic oxidation treatment was conducted under potentiostatic control and the measurement was made in an electrolyte solution consisting of $NH_4F$:$H_2O$:glycerol at a ratio of 1:20:79 wt.% in a glass chamber using a direct-current power supply system (SP6306, Samwoo Elect., Siheung, Korea). The voltage and current density were 20 V and 30 mA/cm$^2$, respectively, and applied for 1 h at room temperature. The nanotube structure on Ti was analyzed via field emission scanning electron microscopy (FE-SEM) using a SUPRA40VP apparatus (Carl Zeiss, Oberkochen, Germany). Pure and Ti nanotubes with dimensions of 1 × 1 cm × 1 mm and 6 × 6 cm × 1 mm, respectively, were used *in vitro*, and pure and Ti nanotube miniature screws with a length of 4.5 mm and a diameter of 0.85 mm were used for *in vivo* dental implants. The preparations were cleaned with deionized water before loading with KRGEs.

### 2.2. Loading of KRGEs

In this experiment, the KRGEs were loaded on to both a P-Ti plate and a miniimplant specimen, on which a $TiO_2$ nanotube layer was formed. The KRGE was prepared by mixing an extract of 100% 6-year-old Korean Red Ginseng root (ginsenoside Rg1 + Rb1 4.5 mg/g, Korea Ginseng Co., Daejeon, Korea) and distilled water, in the ratio 1:2. Each Ti surface was immersed in diluted KRGE solution of the 24-well plate, incubated under stirring on a shaker (Jeio Tech, SK-300, Daejeon, Korea) for 24 h, and dried under nitrogen gas. Finally, each specimen was sterilized in ethylene oxide gas (100% EO Gas Sterilizer, standard type, HS-4313EO, Hanshin Medical Co., Ltd., Incheon, Korea) (MC-3671, Castle, USA). The codes and conditions used in this experiment are listed in Table 1.

**Table 1**
Experimental codes and conditions

| Code | Conditions |
|---|---|
| NC | Without pure titanium |
| P-Ti | Pure titanium |
| N-Ti | Titanium nanotube |
| GN-Ti | Korea Red Ginseng extract–loaded titanium nanotube |

### 2.3. Measurement of surface properties of Ti nanotubes loaded with KRGEs

The nanotubes and KRGE-loaded specimens were coated with an osmium coater (HPC-1SW, Vaccum Device Inc., Mito City, Japan), and their morphologies were analyzed using FE-SEM (S-4800, Hitachi, Japan).

For assessment of surface hydrophobicity and hydrophilicity, surface wettability was measured by dropping 10 μl of distilled water onto the surface from a point 5 cm away. The shape of the formed water drop was photographed using a DE/EZ 4 stereoscopic microscope (Leica Microsystems, Wetzlar, Germany), and the contact angle was measured using the National Institutes of Health ImageJ software.

### 2.4. In vitro experiment

#### 2.4.1. Cell culture

MC3T3-E1 cells (CRL-2593; American Tissue Type Collection, Manassas, VA, USA), were used, a mouse osteoblast precursor cell line derived from *Mus musculus* calvaria, cultured in α-MEM (minimum essential medium) (Gibco BRL, Grand Island, NY, USA) supplemented with 10% fetal bovine serum, 2 mM glutamine, 100 units/mL of penicillin, and 100 μg/mL of streptomycin, maintained at 37°C in a humidified 5% $CO_2$ incubator, and subcultured at a ratio of 1:4. The medium was replaced every 3 days, and cells were used when they reached 80% confluence. For cell differentiation, cells were cultured for 7 days in a differentiation media additionally supplemented with 50 μg/mL of ascorbic acid, 10 mM β-glycerophosphate, and 100 nM dexamethasone.

#### 2.4.2. 3-(4,5-dimethylthiazol-2-yl)-2,5-diphenyltetrazolium bromide assay

3-(4,5-dimethylthiazol-2-yl)-2,5-diphenyltetrazolium bromide (MTT; Sigma-Aldrich Co., St Louis, MO, USA) assays were conducted to determine the proliferation of cells loaded on to the untreated P-Ti plate, N-Ti, and GN-Ti (Table 1); the MC3T3-E1 cells ($2.0 \times 10^4$ cells/well) in a 24-well culture plate were seeded on the P-Ti, N-Ti, and GN-Ti specimens. Cells were incubated for 1–3 days in the presence of 5% $CO_2$. After 1- and 3-day periods, the medium was removed, and the MTT solution was diluted to a ratio of 1:9 (v/v) in fetal bovine serum (FBS)-free α-MEM, followed by the addition of 1 ml MTT diluent to each specimen for 4 h. The cells were loaded on to a 96-well plate in a 200 μL formazan solution, and the optical density was measured at 540 nm using an enzyme-linked immunosorbent assay (ELISA) reader (Model SpectraMax Plus, Molecular Devices, Sunnyvale, CA, USA).

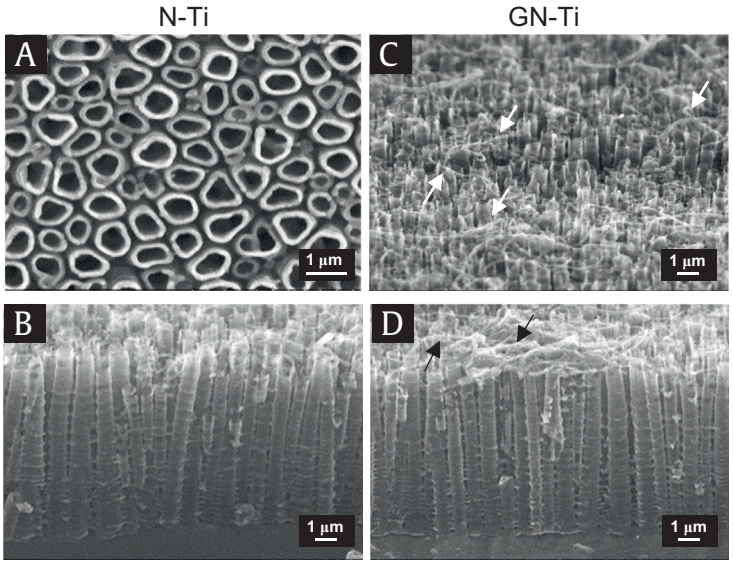


**Fig. 1.** Field emission scanning electron microscope (FE-SEM) images of fabricated nanotube structure. (A) Frontal view of the control N-Ti. (B) Lateral view of the control N-Ti. (C) Frontal view of the GN-Ti. (D) Lateral view of the GN-Ti. Size marker, 1 μm.
GN-Ti, Korea Red Ginseng extract–loaded titanium nanotube; N-Ti, titanium nanotube.

*2.4.3. Alkaline phosphatase activity assay*

Cell differentiation was determined by the alkaline phosphatase (ALP) activity assay. The MC3T3-E1 cells ($2.0 \times 10^4$ cells) seeded on the P-Ti, N-Ti, and GN-Ti implant specimens were cultured in differentiation media for 7 days. The culture medium was removed and washed with a phosphate-buffered saline (PBS) solution, followed by treatment of each specimen with 200 μL of lysis buffer (10 mM Tris-HCl, magnesium chloride 2mM, 0.1% Triton X−100, pH 7.4). After centrifugation at 4°C for 10 min at 2,500 ×g, 20 μL of the supernatant was mixed with 100 μL of para-nitrophenyl phosphate ALP solution. The optical density was measured at 450 nm using an ELISA reader (Model SpectraMax Plus, Molecular Devices).

*2.4.4. Crystal violet staining*

KRGE-induced morphologic changes in MC3T3-E1 cells were determined via crystal violet staining. MC3T3-E1 cells ($2.0 \times 10^4$ cells) seeded on the P-Ti, N-Ti, and GN-Ti specimens were cultured for 3 days, and the cultured media were depleted and washed with PBS. The cells were fixed in PBS-containing 0.2% glutaraldehyde and 3% formaldehyde and then stained with 0.3% crystal violet. The morphological structure of the stained live cells was observed using an optical microscope (Leica DM2500).

*2.5. In vivo experiment*

*2.5.1. Animals and surgical procedures*

Eight-week-old Sprague Dawley (SD) rats were used for the *in vivo* experiments. The study protocol was approved by the Animal Experiment Ethical Committee of Jeonbuk National University. All surgical procedures were performed under veterinary supervision; the rats were placed under general anesthesia, induced with ketamine (ketamine hydrochloride, Yuhan Co., Seoul, Korea) and xylazine hydrochloride (Rompun; Bayer Korea, Seoul, Korea). The lower first molar was carefully extracted to avoid damage to the extraction socket. After 4 weeks of healing, implantation was conducted.

The rats were divided into two groups: the control group, that is, the N-Ti specimens (n = 10), and the GN-Ti (n = 10). The implant sites were prepared using a 0.8 mm diameter drill operated at a low speed of 900 rpm, using saline irrigation to avoid heating. The implants were inserted in these sites, and implantation was considered successful when, at the end of the experimental period, the implant showed no signs of mobility in situ. All rats were reared in individual cages, with the temperature maintained at 20–25°C and relative humidity at 30–50%. Postoperative antibiotic treatment was administrated according to body weight via daily injection for 4 days.

*2.5.2. Microcomputed tomography analysis*

Changes in the tissue around the implant were analyzed using microcomputed tomography (μ-CT) (Skyscan, model 1076 apparatus, Kontich, Belgium). The μ-CT was performed by operating with an anode electrical current of 100 kV, at a resolution of 18 μm. After implantation, at 2 and 4 weeks, the rats in each group were anesthetized and the mandibles were scanned by μ-CT to evaluate the dynamic changes in the periimplant tissue. The regions of interest (ROIs) including the mandible compartment around the implant were selected. After scanning, three-dimensional (3D) models were generated by CTVol (Skyscan), which was further used to examine the μ-CT data sets for new bone growth. The volume of interest in the regenerated bone consisted of the collective sum of all ROI layers over a continuous set of cross-sectional (lateral) image slices. Furthermore, new bone volume and bone mineral density around the implant were calculated based on μ-CT images of the phantoms, followed by calculation of the Hounsfield units (HU). The bone and implant threshold value was determined between low (0.25) 1089.7966 HU and high phantom (0.75) 3241.0643 HU. The presence or absence of bone volume was determined based on this threshold. As the volume of the ROI corresponds to the volume of the original bone, the amount of bone present within the ROI is considered to be the newly formed bone. To create 3D images, binary thresholds were selected (a gray scale index, with implant: 160 × 255 mm; new bone: 100 × 143 mm; total bone: 70 × 120 mm).

*2.5.3. Histology staining and immunohistochemical staining*

The mandibles with the implants were isolated and fixed in 10% neutral-buffered formalin solution. After decalcification in 15%

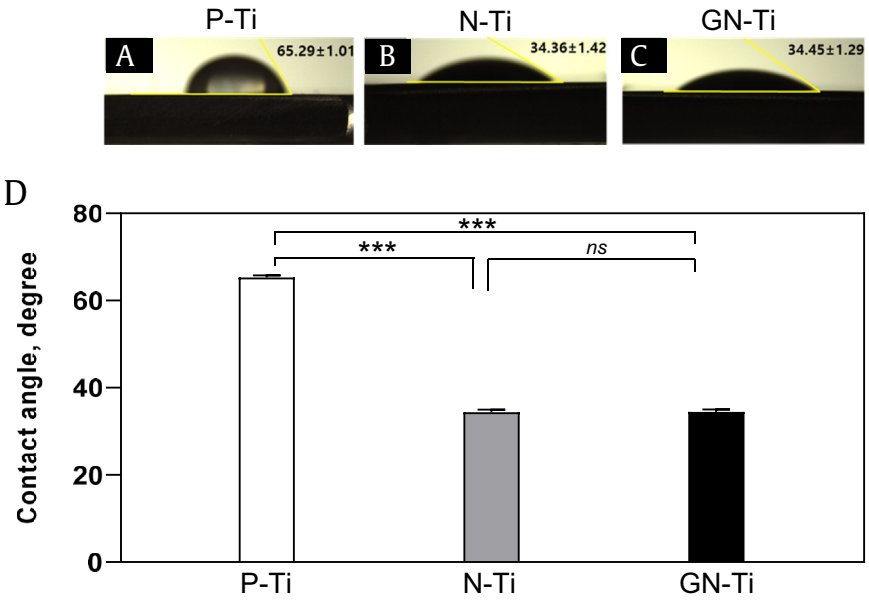


**Fig. 2.** Changes in the wettability of Ti specimens coated with diverse materials. (A) Contact angle of the surface droplet on the untreated pure Ti (P-Ti) plate. (B) Contact angle of the surface droplet on the N-Ti. (C) Contact angle of the surface droplet on the GN-Ti. (D) Bars depict the average contact angle of the surface for various types of Ti specimens. Data are shown as mean ± SE, unless otherwise mentioned (n = 5; *ns*; not significant; ***$P < 0.001$, P-Ti *vs.* N-Ti or GN-Ti).
GN-Ti, Korea Red Ginseng extract–loaded titanium nanotube; N-Ti, titanium nanotube.

ethylenediaminetetraacetic acid and 0.1 M Tris (pH 7.0), the implants were gently removed, and the mandibular tissues were dehydrated, cleared, and embedded in paraffin. Tissue sections, 8 mm in thickness, were mounted on glass slides and subjected to immunohistochemical (IHC) and hematoxylin and eosin (H&E) staining. IHC staining was performed to detect the expression of bone morphogenesis protein (BMP)-2, BMP-7, and collagen, using the immunohistochemistry accessory kit (Bethyl Laboratories, Montgomery, TX, USA). Collagen analysis was performed via Masson's trichrome staining using a commercial kit (Masson's trichrome stain kit, Sigma-Aldrich). The primary antibodies of BMP-2 (BMP2 P275 pAb, Bioworld Technology, Inc., USA) and BMP-7 (BMP7 E173 pAb, Bioworld Technology) were diluted in the ratio 1:100 for 30 min at room temperature in accordance with the manufacturer's protocol. The stained specimens were visualized microscopically (Carl Zeiss, Oberkochen, Germany) and cell counts in the newly formed bone area were obtained, in a 0.5 mm area surrounding the implants.

### 2.6. Statistical analysis

The experimental data of every group were analyzed using one-way analysis of variance to determine the differences in the variables among the groups. The post-hoc test was performed using the Tukey test, and *P*-values $< 0.05$ were considered statistically significant.

## 3. Results

### 3.1. Establishment and characteristics of the N-Ti plate for drug loading

The goal of this study is to improve mechanical, chemical, and physical properties of metallic biomaterials for dental implantation and stabilization of implants. The specimens were prepared from P-Ti plates. The nanotube structure was fabricated on P-Ti via anodic oxidation, using a voltage of 20 V for 1 h. The surface morphology of the nanotube structure was dense and uniform on the entire surface of the plate (Fig. 1A). In particular, the frontal and lateral views of the N-Ti plate indicated the formation of tubular structures, with an open and enlarged shape containing multiple empty volumes (Fig. 1A and B); these played a key role in maximum efficiency of drug absorption when the drug was loaded. As expected, after KRGE loading of the N-Ti, the needle-like particles formed over the surface and the underlying nanotubes were not visible (Fig. 1C and D).

The surface contact angle was measured to assess the hydrophobicity and hydrophilicity of the different surfaces; the contact angle of water on the P-Ti surface was 65.29°, indicating hydrophobic behavior (Fig. 2A and D). However, the N-Ti and GN-Ti surfaces demonstrated hydrophilic behavior, indicated by a decrease in the contact angle to 34.36° and 34.45°, respectively (Fig. 2B–D). This change in the contact angle suggests that the hydrophilicity of the surface was significantly improved by anodization of the Ti plate (Fig. 2, ***$P < 0.001$ *vs* Ti). However, the KRGE loading itself did not alter the surface contact angle of the N-Ti.

Furthermore, construction of a miniimplant specimen via coating with the GN-Ti for the *in vivo* study and visualization by FE-SEM revealed that the N-Ti with a diameter of 60~90 nm on the miniimplant specimen showed structural and morphological patterns similar to the N-Ti shown in Fig. 1 (Fig. 3).

The overall results suggest that the synthesis of nanotubes on the P-Ti plate alters the physical and chemical properties, thus facilitating effective absorption of the surface materials for implant stabilization.

### 3.2. Effects of KRGE treatment on morphology, proliferation, and differentiation of mouse osteoblasts

To investigate the effect of KRGE loading on MC3T3-E1 cells seeded on the P-Ti and N-Ti surfaces, the cell viability was assessed using the MTT and crystal violet staining assay. For the experiment, MC3T3-E1 cells were cultured on various types of Ti, with either a

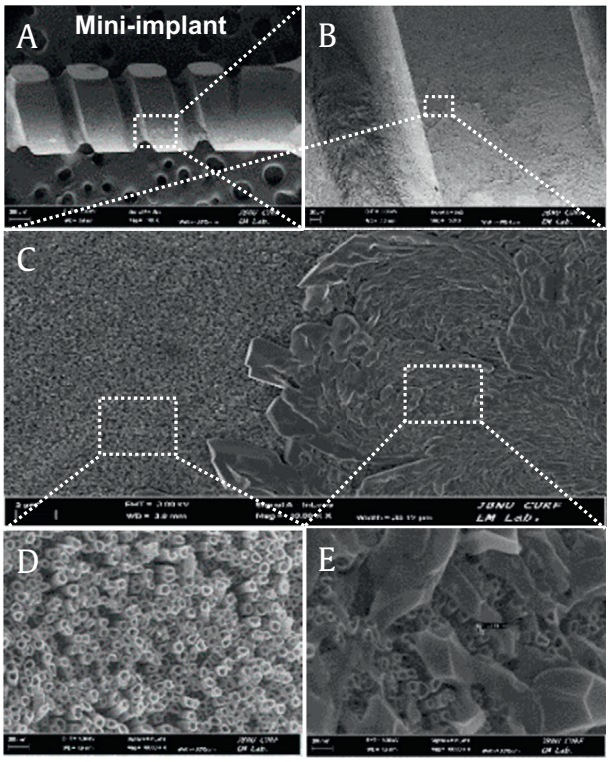


**Fig. 3.** FE-SEM images of the GN-Ti on the miniimplant. (A) Image of the GN-Ti miniimplant. (B) Enlarged image of the square box with white dot in (A). (C) Enlarged image of a white square in (B). (D) and (E) enlarged images of different location in the white squares indicated in (C).
GN-Ti, Korea Red Ginseng extract–loaded titanium nanotube; N-Ti, titanium nanotube; FE-SEM, field emission scanning electron microscopy.

vehicle or KRGE, and their effects on cell growth and proliferation were measured on days 1 and 3 after culturing. MC3TC-E1 cells cultured for 3 days on the GN-Ti showed a more dramatic increase in proliferation than the cells cultured on P-Ti or the KRGE-depleted N-Ti (Fig. 4B, $^{***}P < 0.001$). However, none of the three groups showed significant changes in cellular proliferation after short-term (1 day) culture (Fig. 4A). Interestingly, MC3T3-E1 cells displayed slightly promoted cell growth, despite the P-Ti surface (Fig. 4B, $^{*}P < 0.05$ *vs* negative control (NC) or N-Ti treatment group).

Similarly, the cell morphology on P-Ti was evaluated microscopically using a crystal violet staining assay (Fig. 4C). MC3T3-E1 cells incubated on the GN-Ti showed a highly dense morphology compared with those on P-Ti or the N-Ti without KRGEs (Fig. 4D; the white dotted areas).

The trend observed in the ALP assay is quite similar to the one inferred from the MTT assay. The ALP activity assay to detect the degree of osteoblast differentiation after MC3T3-E1 cells cultured for 7 days revealed that the degree of cell differentiation was much higher on the GN-Ti (Fig. 4C, $^{*}P < 0.05$). However, no significant difference in the ALP activity of NC, P-Ti, and the N-Ti could be observed (Fig. 4C).

Although the underlying cellular and molecular mechanisms have yet to be defined, our *in vitro* studies with osteoblast cell lines collectively clearly show that the KRGE affects the morphology, differentiation, and viability of osteoblast-like cells.

### 3.3. Effects of the GN-Ti on new bone formation and bone mineral density in a rat mandible

Based on previous morphological observations shown in Figs. 1 and 3, we confirmed that the N-Ti plates can be effectively loaded with diverse target molecules. In addition, incorporation of KRGEs on to the N-Ti plates greatly enhanced the proliferation and differentiation of cells. The final goal of this study, however, was to determine whether the KRGE plays a role in successful integration of the implanted specimens with tissues around the implant. Therefore, we performed an *in vivo* study after fabricating the KRGE-loaded N-Ti miniimplant specimens, as described in Materials and methods section.

First, we examined whether the nanotube surface and pharmacological activity of KRGEs influenced bone formation in a rat mandible after implantation. For the *in vivo* implantation in SD rats, the lower first molar was extracted, and a 4-month period was allowed for complete healing. μ-CT analysis was carried out for structural and quantitative assessments of new bone formation and mineralization in the defective site after implantation. μ-CT is also very useful for identifying a suitable implant site and assessing the newly restored bone. Two-dimensional (2D) μ-CT images showed the morphology of the tooth before and after extraction, and the bone restoration at the extraction site was completely healed (Fig. 5A, white arrow). Therefore, at 4 weeks after tooth extraction, N-Ti and GN-Ti implants were inserted into the healing site of the mandible. Four weeks after implantation, 2D μ-CT images revealed the successful anchorage of the GN-Ti implants but not the N-Ti implants (Fig. 5B). This result was further confirmed by the 3D μ-CT images, which clearly indicate an increase in the extent of new bone formation (pink) on the GN-Ti implant (gray in upper panel of the GN-Ti) compared with that formed on the N-Ti implant (gray in upper panel of N-Ti, Fig. 5C). Furthermore, the volume of the newly formed bone and bone mineral density was significantly enhanced around the GN-Ti surface than around the N-Ti surface at 4 weeks after implantation (Fig. 6A and B). The differences in new bone formation were apparent by 1 week after implantation and remained so for 4 weeks (Fig. 6A), while the difference in bone mineral density was observed at 2 weeks after implantation (Fig. 6B). These results are quite plausible as bone density gradually increases after initial bone formation.

### 3.4. Effects of the N-Ti loaded with KRGEs on new bone formation and bone mineral density in a rat mandible

Four weeks after implantation, new bone formation around both the N-Ti and GN-Ti implants was assessed via Masson's trichrome and H&E staining. Masson's trichrome staining indicated the limited formation of collagen fibers around the surface of the N-Ti implant (Fig. 7A). The newly formed bone around this implant surface was the immature bone with little growing of bone surrounding the implant (Fig. 7C and D). In addition, loosely organized, inflammatory infiltrate, and irregular bone trabeculae, with a limited number of osteoblasts, were observed on the N-Ti implants. In contrast, Masson's trichrome staining showed well-formed collagenous bone trabeculae and muscle fibers and cytoplasm, marked in blue and red, respectively (Fig. 7B). Furthermore, a relatively well-formed new bone with regular bone trabeculae was observed at implant sites around the GN-Ti (Fig. 7E and F).

### 3.5. Effects of the N-Ti loaded with KRGEs on bone morphogenesis and protein expression in a rat mandible

The expression of BMP-2 and BMP-7 was examined for osteogenic differentiation on surfaces with both the N-Ti and GN-Ti, after 4 weeks of implantation. The dark brown cells in the square dotted box indicate the expression of BMP-2 and BMP-7 (Fig. 8). Expression of BMP-2 and BMP-7, the markers for osteogenic differentiation via IHC staining, was more intense around the GN-Ti surface than around the N-Ti surface (Fig. 8B and D).

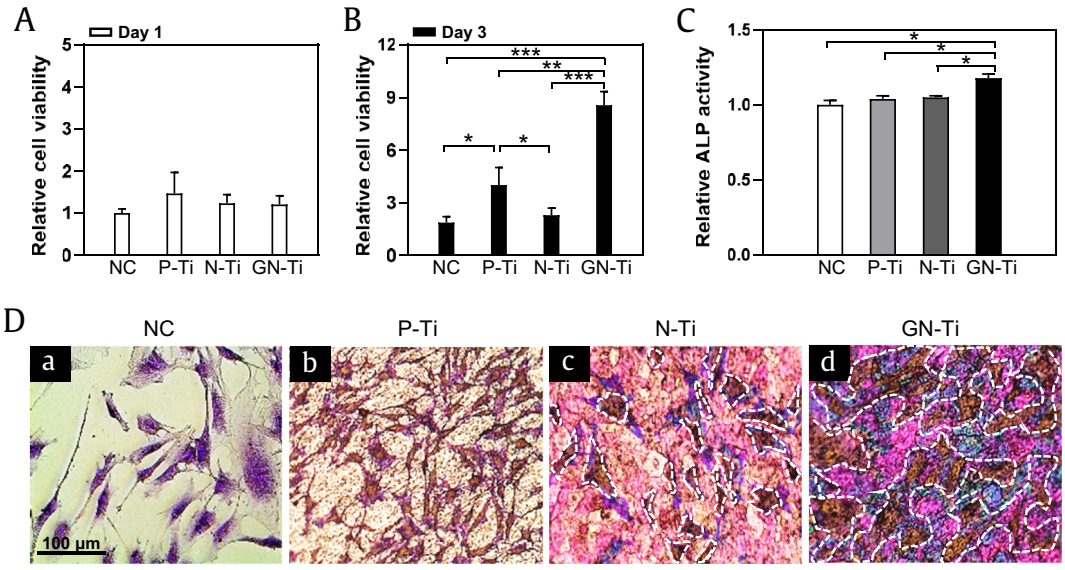


**Fig. 4.** Viability and morphology of MC3T3-E1 cells seeded on different Ti surfaces coated with various materials. (A, B) Relative quantification of proliferation, (C) differentiation, and (D) morphology of MC3T3-E1 cells cultured on NC, on untreated pure Ti (P-Ti), the N-Ti, and GN-Ti. Cellular proliferation and differentiation were performed by MTT and ALP activity assays, respectively. Cells were cultured for 1-3 days for the MTT assay and for 7 days for ALP activity assay. Cell morphology was visualized by crystal violet staining after culturing for 3 days (mean ± SE, n = 5; $*P < 0.05$, $**P < 0.01$, and $***P < 0.001$; day 1 *vs.* day 3 in each treatment group). The size bar, 100 μm.
MTT, 3-(4,5-dimethylthiazol-2-yl)-2,5-diphenyltetrazolium bromide; ALP, alkaline phosphatase; GN-Ti, Korea Red Ginseng extract–loaded titanium nanotube; N-Ti, titanium nanotube.

## 4. Discussion

In this study, we elucidated the effect of KRGEs on osseointegration and new bond formation, after implantation. Accordingly, the miniimplant specimen was subjected to the surface treatment to improve the properties of metallic biomaterials, such as abrasion resistance, corrosion resistance, biocompatibility, and surface energy. Today, major dental implants comprise commercial P-Ti or Ti alloys, for example, Ti-6AI-4V; P-Ti was used for this study. In detail, the Ti plate was fabricated via a simple anodization technique, using an anodization voltage of 20 V and a current of 30 mA/cm$^2$ for 1 h, obtaining a nanotube structure with a pore size of approximately 50 ± 15 nm and length of 1.26 μm, which was subsequently loaded with KRGEs. Analysis of the top and cross-sectional surfaces of the specimen revealed a uniform distribution of the N-Ti both on the P-Ti plate and miniimplant, indicating that many of the nanotubes displayed the cross-sectional shape of an empty tube. This structural morphology of the miniimplant surface may facilitate packing bioactive materials inside the empty tubes, as evidenced by the scanning electron microscope (SEM) images of the KRGE-loaded specimen, which showed that the surfaces of the nanotubes were evenly covered with KRGE particles.

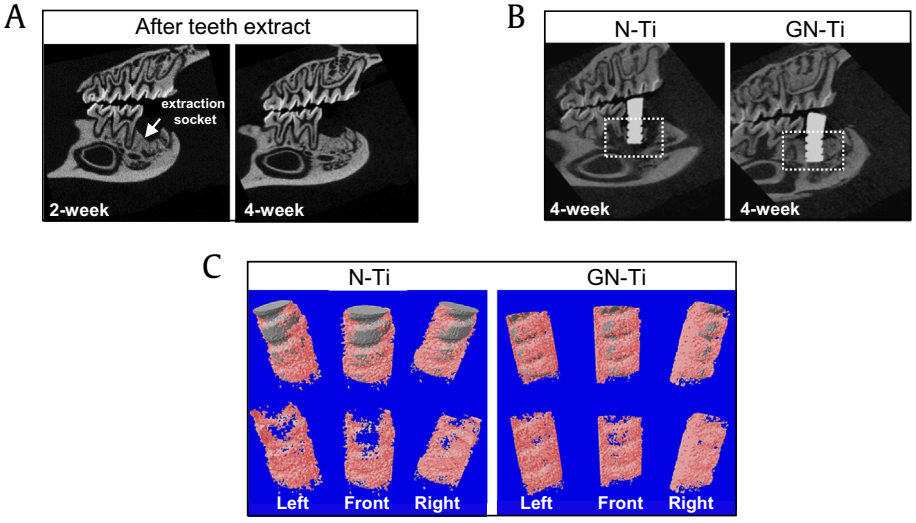


**Fig. 5.** μ-CT analytical images of periimplant bone tissues after 4 weeks of implantation in the healed mandibular edentulous site of the rat. (A, B) Two-dimensional (2D) and (C) 3D μ-CT images of bone tissues. In the *in vivo* model, lower first molars of SD rats were extracted, and the extraction site was allowed to heal for a duration of 2 and 4 weeks (A) and the changes in the periimplant tissue and position of N-Ti and GN-Ti implants were determined at 4 week via 2D μ-CT monitoring (B). After 4 weeks, the thickness of the newly formed bone surrounding the implant was determined by 3D μ-CT; gray represents the implant and pink depicts the bone tissue (C) (n = 10, each group).
μ-CT, microcomputed tomography; SD, Sprague Dawley; 3D, three-dimensional; GN-Ti, Korea Red Ginseng extract–loaded titanium nanotube; N-Ti, titanium nanotube.

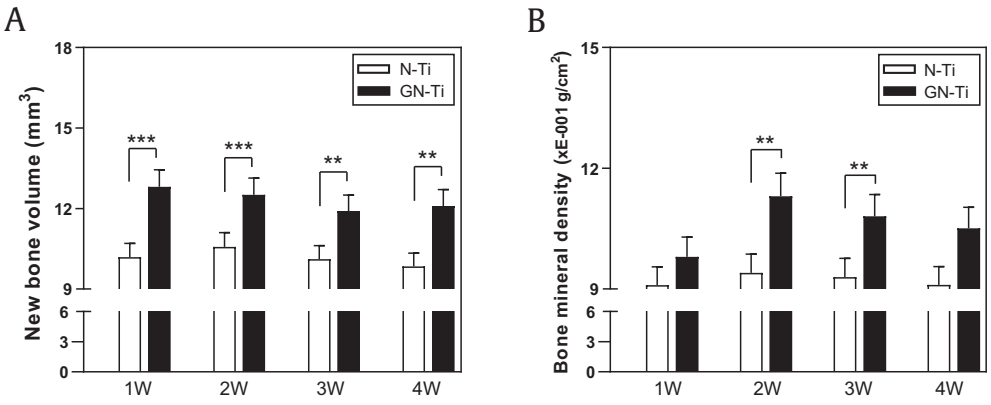


**Fig. 6.** Periimplant bone scan for new bone volume and bone mineral density analysis. (A) New bone volume and (B) bone mineral density were measured by 3D μ-CT analysis from week 1 to 4 after implantation. In the *in vivo* model, lower first molars of SD rats were extracted. When the extraction site was healed, the bone tissue around the N-Ti and GN-Ti implants was scanned weekly (mean ± SE, n = 10; $^{**}P < 0.01$ and $^{***}P < 0.001$, N-Ti *vs*. GN-Ti at each week).
N-Ti, titanium nanotube; GN-Ti, Korea Red Ginseng extract–loaded titanium nanotube; SD, Sprague Dawley; 3D, three-dimensional; μ-CT, microcomputed tomography.

Several studies have investigated surface wettability, effects of electric charge, and the shape and amount of proteins adsorbed onto Ti surfaces [17]. Furthermore, some recent studies have reported that cell attachment and proliferation are more active on hydrophilic, positively charged amine surfaces compared with hydrophobic surfaces [18–20]. Via dropping an analogous fluid on the surfaces of a home-made specimen, we measured the surface contact angle of the N-Ti to be greatly reduced (to almost half a degree), when compared with the contact angle of P-Ti, thus implying improved hydrophilicity. Interestingly, KRGE loading onto the N-Ti did not alter its surface wettability, further suggesting an increase in hydrophilicity. The results demonstrated that the N-Ti is a suitable vehicle for the loading and sustained elution of chemicals and biomolecules [21,22]. There are consistently a significant number of reports that hydrophilic surface promotes the ready attachment of cells [16,21].

The success of dental implants depends on multiple factors that act during the sequential stages of osseous healing, after implant placement. Osseointegration suggests a structural and functional connection between the living bone and surface of a load-bearing artificial implant. During osseointegration, after dental implantation, two factors influence implant stability [23]: the implant surface structure and composition affect the attachment of proteins and subsequent cellular processes associated with implant osseointegration and the implant stability is affected by the stimulator of bone formation.

In this study, compared with cells on the nonloaded N-Ti, MC3T3-E1 cells cultured on the GN-Ti presented a significant increase in cell viability at 3 days *in vitro* and in ALP activity at 7 days *in vitro*. ALP, produced mainly in osteoblasts, is an important component and an early biochemical marker of hard tissue formation, osteoblast differentiation, and bone mineralization [24]. It

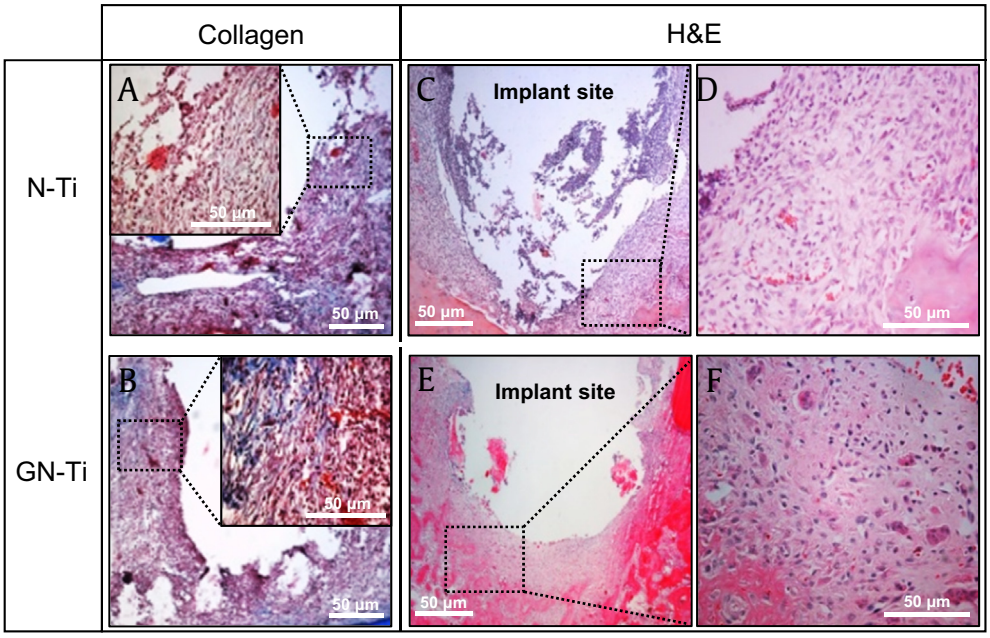


**Fig. 7.** Histomorphological analysis by Masson's trichrome and hematoxylin & eosin staining. Images depict the KRGE-induced expression of collagen and the new bone formation around the implants. Surface bone tissues around (A, C, D) the N-Ti implant and (B, E, F) GN-Ti implant. (D, F) Enlarged image of the black square box with a dot in (C) and (E), respectively. (A, B) Expression of collagen (blue areas) and (C, D, E, F) new bone formation, at 4 weeks after implantation. At least five slides of each specimen were observed. Size marker, 50 μm.
N-Ti, titanium nanotube; GN-Ti, Korea Red Ginseng extract–loaded titanium nanotube; KRGE, Korea Red Ginseng extract.

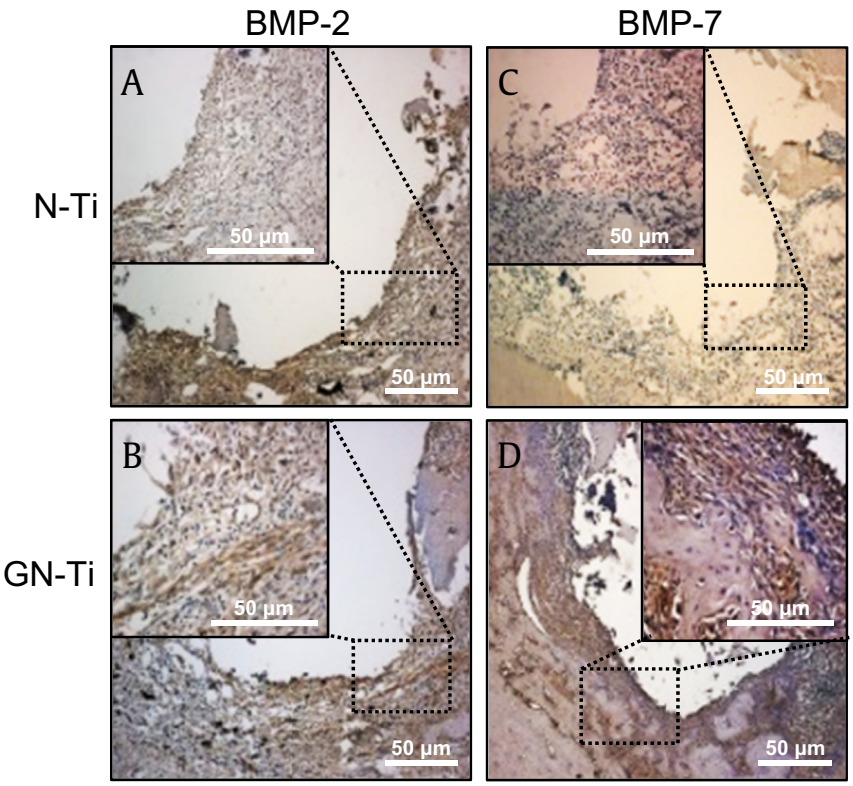


**Fig. 8.** Effect of KRGE loading onto the surface of Ti nanotube implants on the expression of BMP-2 and BMP-7. Four weeks after implantation with the N-Ti, the expressions of BMP-2 (A, B) and BMP-7 (C, D) were analyzed by immunohistochemistry. The brown color indicates positive cells at 4 weeks after implantation. Each black square dot box was enlarged in the black box inside the individual images. Size bars, 50 μm.
BMP-2, bone morphogenesis protein-2; BMP-7, bone morphogenesis protein-7; N-Ti, titanium nanotube; KRGE, Korea Red Ginseng extract.

increases the local concentration of inorganic phosphate, which promotes mineralization and decreases the concentration of extracellular pyrophosphate, which inhibits mineral formation [25]. In addition, ALP is usually abundant in matrix vesicles, which play a role in extracellular matrix processing and bone calcification. During osteogenesis, osteoblasts and osteoblast precursors exhibit high levels of ALP activity on the surface of cytoplasmic membranes, which ultimately contribute to the initiation of mineralization and advanced growth of hydroxyapatite crystals [25]. Thus, increased ALP activity in MC3T3-E1 cells suggests ongoing positive cellular phenotypic changes immediately before bone mineralization, as shown in the crystal violet staining of the cells cultured on the GN-Ti.

To ensure implant stability, a diverse inflammatory reaction and osteogenesis for solid osseointegration formation in the early stage of implantation are important. Bone remodeling occurs throughout life via synthesis of the bone matrix due to the action of osteoblasts and osteoclasts. The appropriate functioning of these cells is necessary to maintain bone mass and bone mineral density. Our *in vivo* study of rats after extracting the first mandibular molar reproduced *in vitro* results, that is, when the specimen was implanted after one month of extraction and the degree of tissue mineralization and new bone formation analyzed by μ-CT at 4 weeks after implant placement, the KRGE-loaded miniimplant showed higher new bone formation and bone density than the vehicle-loaded miniimplant. H&E staining in this study consistently indicated that the new bones were tightly formed in the KRGE-loaded miniimplant, while the new bones formed around the N-Ti miniimplant without loading with KRGEs showed immature bone tissues.

Connective tissue cells, including fibroblasts, cartilage cells, and bone cells, are specialized for the secretion of a collagenous extracellular matrix and are jointly responsible for the architectural framework of the body, thus affecting cell shape and attachment [3]. Masson's trichome staining was further used to detect the expression of collagen secreted in the process of bone formation, which was used as an indirect index of the amount of newly formed bone. Collagen is the main organic matrix protein of the bone, comprising approximately 90%, and is synthesized and secreted by differentiated osteoblasts, which are arranged in a continuous layer on the surface of the bone matrix [26]. Secreted collagen functions as a block structure and the major protein framework for weaving an elaborate bone matrix, thus, ultimately contributing to bone matrix mineralization. In this study, Masson's trichome staining indicated the expression of well-formed collagen fibers around the GN-Ti implants, demonstrating that the surface of these implants enhanced collagen fiber fabrication to form the basic framework of the bone. However, in the case of the N-Ti implants, a limited number of collagen fibers were observed.

Osteoblast differentiation mainly occurs via either Wnt canonical or BMP pathways [27]. BMP-2 and BMP-7 are essential in osteoblastogenesis, such as for the formation and regeneration of the bone. For instance, the transmembrane-bound BMP-2 phosphorylates the Type I receptor and activates the Smad complex signaling pathways, which facilitate the activation of osteoblast-specific transcriptional genes involved in the regulation of bone formation, bone repair, and osseointegration [28–30]. Moreover, overexpression of both BMP-2 and BMP-7 induced high ALP activity in the stromal cells of mice, with more rapid formation of the ectopic bone than in animals with single-gene transfer [31].

Immunostaining of the rat tissue in our *in vivo* study revealed that compared with the vehicle-loaded control group, the KRGE strongly stimulated the expression of BMP-2 and BMP-7 around the implanted site. In addition to KRGEs, statin-coated implants induced BMP-2 expression and promoted osteoblastic BMP signaling [32].

Ginseng has been studied extensively since its discovery. *Panax ginseng* Meyer, commonly known as Korean Red Ginseng, belongs to the family Araliaceae and contains a variety of active ingredients, including ginsenosides, polysaccharides, peptides, polyacetylenic alcohols, and fatty acids [9]. Major active ingredients of ginseng are ginsenosides, which are a class of natural product steroid glycosides and triterpenoids. Ginsenosides contain more than 30 different compounds. Based on their chemical structure, these can be classified into two groups. The first is protopanaxadiols, including Rb1, Rb2, Rg3, Rh2, and Rh3, and the second is protopanaxatriols, including Rg1, Rg2, and Rh1 [33]. Ginseng exhibits antioxidant, anticancer, antidiabetic, antiadipocyte, and sexual enhancement properties [34–36]. Very few studies, however, have investigated its antiosteoporotic activity [27,37,38]. For instance, studies have reported that the ginsenoside Rb1 and Rg1 may alleviate osteoporosis by regulating the expression of osteoprotegerin, a receptor activator of NF-kB ligand (RANKLe), *in vitro* experiment; furthermore, it may promote bone marrow mesenchymal stem cell differentiation toward mature functional osteoblasts by enhancing the Runt-related transcription factor 2 expression [14,39,40]. The effect of Rg1 on osteogenic differentiation of bone marrow mesenchymal stem cells is especially regulated by BMP-2/SMAD signaling [39]. Similarly, the effects of ginsenoside Rg3 and Re on osteoblast differentiation and mineralization in preosteoblastic MC3T3-E1 cells have also been reported [15,41]. In these literatures, Rg3 and Re stimulated osteocalcin, ALP, and collagen secretion, thus accelerating the extracellular matrix mineralization. Furthermore, ginsenoside Rh2 induces the differentiation and mineralization of MC3T3-E1 cells and their molecular mechanism, through the activation of PKD/p38 MAPK (protein kinase D/p38 mitogen-activated protein kinase) pathways [42]. There are many reports that a variety of ginsenoside are associated with osteogenesis and osteoporosis; however, studies on the detailed genetic and molecular action mechanisms require further elucidation.

In this study, we also used KRGEs composed of Rb1 and Rg1 (4.5 mg/ml) and determined that these ingredients can improve the prognosis after dental implantation. The main proteins affected by KRGE loading were BMP-2/7, ALP, and collagen, which are all related to osseointegration. Although an understanding of the molecular working mechanism of KRGEs in the bone biology after dental implantation is still required, our results suggest that the GN-Ti can be effectively used for clinical applications as little is known about the specific effective ingredients of Korean Red Ginseng concerning dental implantation; we will present the detailed mechanisms in a follow-up study.

## Conflicts of interest

All contributing authors declare no conflicts of interest.

## Acknowledgments

This research was supported by Basic Science Research Program through the National Research Foundation of Korea (NRF) funded by the Ministry of Education (2016R1D1A1B04934383). It was also supported by Jeonbuk National University, Republic of Korea.

## References

[1] Oshida Y, Tuna EB, Aktoren O, Gencay K. Dental implant systems. Int J Mol Sci 2010;11:1580–678.
[2] Adell R. Tissue integrated prostheses in clinical dentistry. Int Dent J 1985;35:259–65.
[3] Miao X, Wang D, Xu L, Wang J, Zeng D, Lin S, Huang C, Liu X, Jiang X. The response of human osteoblasts, epithelial cells, fibroblasts, macrophages and oral bacteria to nanostructured titanium surfaces: a systematic study. Int J Nanomedicine 2017;12:1415–30.
[4] Park J, Bauer S, von der Mark K, Schmuki P. Nanosize and vitality: TiO2 nanotube diameter directs cell fate. Nano Lett 2007;7:1686–91.
[5] Das K, Bose S, Bandyopadhyay A. TiO2 nanotubes on Ti: influence of nanoscale morphology on bone cell-materials interaction. J Biomed Mater Res A 2009;90:225–37.
[6] Lee YH, Bhattarai G, Park IS, Kim GR, Kim GE, Lee MH, Yi HK. Bone regeneration around N-acetyl cysteine-loaded nanotube titanium dental implant in rat mandible. Biomaterials 2013;34:10199–208.
[7] Brekhman II, Dardymov IV. New substances of plant origin which increase nonspecific resistance. Annu Rev Pharmacol 1969;9:419–30.
[8] Shibata S, Ando T, Tanaka O. Chemical studies on the oriental plant drugs. XVII. The prosapogenin of the ginseng saponins (ginsenosides-Rb1, -Rb2, and -Rc). Chem Pharm Bull (Tokyo) 1966;14:1157–61.
[9] Attele AS, Wu JA, Yuan CS. Ginseng pharmacology: multiple constituents and multiple actions. Biochem Pharmacol 1999;58:1685–93.
[10] Gonzalez-Burgos E, Fernandez-Moriano C, Gomez-Serranillos MP. Potential neuroprotective activity of Ginseng in Parkinson's disease: a review. J Neuroimmune Pharmacol 2015;10:14–29.
[11] Jung JH, Kang IG, Kim DY, Hwang YJ, Kim ST. The effect of Korean red ginseng on allergic inflammation in a murine model of allergic rhinitis. J Ginseng Res 2013;37:167–75.
[12] Wong AS, Che CM, Leung KW. Recent advances in ginseng as cancer therapeutics: a functional and mechanistic overview. Nat Prod Rep 2015;32:256–72.
[13] Bei J, Zhang X, Wu J, Hu Z, Xu B, Lin S, Cui L, Wu T, Zou L. Ginsenoside Rb1 does not halt osteoporotic bone loss in ovariectomized rats. PLoS One 2018;13:e0202885.
[14] He F, Yu C, Liu T, Jia H. Ginsenoside Rg1 as an effective regulator of mesenchymal stem cells. Front Pharmacol 2019;10:1565.
[15] Park CM, Kim HM, Kim DH, Han HJ, Noh H, Jang JH, Park SH, Chae HJ, Chae SW, Ryu EK, et al. Ginsenoside Re inhibits osteoclast differentiation in mouse bone marrow-derived macrophages and Zebrafish scale model. Mol Cells 2016;39:855–61.
[16] Park IS, Lee MH, Bae TS, Seol KW. Effects of anodic oxidation parameters on a modified titanium surface. J Biomed Mater Res B Appl Biomater 2008;84:422–9.
[17] Jacinto A, Wolpert L. Filopodia. Curr Biol 2001;11:R634.
[18] Britland S, Clark P, Connolly P, Moores G. Micropatterned substratum adhesiveness: a model for morphogenetic cues controlling cell behavior. Exp Cell Res 1992;198:124–9.
[19] Georger Jr JHSD, Rudolph AS, Hickman JJ. Coplanar patterns of self-assembled monolayers for selective cell adhesion and outgrowth, thin solid films. Thin Solid Films 1992;210–211:716–9.
[20] Stenger DAGJ, Dulcey CS, Hickman JJ, Rudolph AS, Nielsen TB, McCort SM, Calvert JM. Coplanar molecular assemblies of amino and perfluorinated alkylsilanes: characterization and geometric definition of mammalian cell adhesion and growth. Journal of American Chemical Society 1992;114:8435–42.
[21] Moon SH, Lee SJ, Park IS, Lee MH, Soh YJ, Bae TS, Kim HS. Bioactivity of Ti-6Al-4V alloy implants treated with ibandronate after the formation of the nanotube TiO2 layer. J Biomed Mater Res B Appl Biomater 2012;100:2053–9.
[22] Popat KC, Eltgroth M, Latempa TJ, Grimes CA, Desai TA. Decreased Staphylococcus epidermis adhesion and increased osteoblast functionality on antibiotic-loaded titania nanotubes. Biomaterials 2007;28:4880–8.
[23] Stadlinger B, Korn P, Todtmann N, Eckelt U, Range U, Burki A, Ferguson SJ, Kramer I, Kautz A, Schnabelrauch M, et al. Osseointegration of biochemically modified implants in an osteoporosis rodent model. Eur Cell Mater 2013;25:326–40. discussion 39-40.
[24] Stein GS, Lian JB, Owen TA. Relationship of cell growth to the regulation of tissue-specific gene expression during osteoblast differentiation. FASEB J 1990;4:3111–23.
[25] Golub EE, B-BK. The role of alkaline phosphatase in mineralization. Curr. Opin. Orthopaed. 2007;18:444–8.
[26] Mathews S, Bhonde R, Gupta PK, Totey S. A novel tripolymer coating demonstrating the synergistic effect of chitosan, collagen type 1 and hyaluronic acid on osteogenic differentiation of human bone marrow derived mesenchymal stem cells. Biochem Biophys Res Commun 2011;414:270–6.
[27] Siddiqi MH, Siddiqi MZ, Ahn S, Kang S, Kim YJ, Sathishkumar N, Yang DU, Yang DC. Ginseng saponins and the treatment of osteoporosis: mini literature review. J Ginseng Res 2013;37:261–8.
[28] Balloni S, Calvi EM, Damiani F, Bistoni G, Calvitti M, Locci P, Becchetti E, Marinucci L. Effects of titanium surface roughness on mesenchymal stem cell commitment and differentiation signaling. Int J Oral Maxillofac Implants 2009;24:627–35.

[29] Derynck R, Zhang Y. Intracellular signalling: the mad way to do it. Curr Biol 1996;6:1226–9.
[30] Reddi AH. Bone and cartilage differentiation. Curr Opin Genet Dev 1994;4:737–44.
[31] Kawai M, Bessho K, Maruyama H, Miyazaki J, Yamamoto T. Simultaneous gene transfer of bone morphogenetic protein (BMP) -2 and BMP-7 by in vivo electroporation induces rapid bone formation and BMP-4 expression. BMC Musculoskelet Disord 2006;7:62.
[32] Mundy G, Garrett R, Harris S, Chan J, Chen D, Rossini G, Boyce B, Zhao M, Gutierrez G. Stimulation of bone formation in vitro and in rodents by statins. Science 1999;286:1946–9.
[33] Lu JM, Yao Q, Chen C. Ginseng compounds: an update on their molecular mechanisms and medical applications. Curr Vasc Pharmacol 2009;7:293–302.
[34] Polan ML, Hochberg RB, Trant AS, Wuh HC. Estrogen bioassay of ginseng extract and ArginMax, a nutritional supplement for the enhancement of female sexual function. J Womens Health (Larchmt) 2004;13:427–30.
[35] Shin HY, Jeong HJ, Hyo Jin A, Hong SH, Um JY, Shin TY, Kwon SJ, Jee SY, Seo BI, Shin SS, et al. The effect of Panax ginseng on forced immobility time & immune function in mice. Indian J Med Res 2006;124:199–206.
[36] Wang W, Zhao Y, Rayburn ER, Hill DL, Wang H, Zhang R. In vitro anticancer activity and structure-activity relationships of natural products isolated from fruits of Panax ginseng. Cancer Chemother Pharmacol 2007;59:589–601.
[37] Kim HR, Cui Y, Hong SJ, Shin SJ, Kim DS, Kim NM, So SH, Lee SK, Kim EC, Chae SW, et al. Effect of ginseng mixture on osteoporosis in ovariectomized rats. Immunopharmacol Immunotoxicol 2008;30:333–45.
[38] Kim J, Lee H, Kang KS, Chun KH, Hwang GS. Protective effect of Korean Red Ginseng against glucocorticoid-induced osteoporosis in vitro and in vivo. J Ginseng Res 2015;39:46–53.
[39] Gu Y, Zhou J, Wang Q, Fan W, Yin G. Ginsenoside Rg1 promotes osteogenic differentiation of rBMSCs and healing of rat tibial fractures through regulation of GR-dependent BMP-2/SMAD signaling. Sci Rep 2016;6:25282.
[40] Li J, Wang Q, Yang R, Zhang J, Li X, Zhou X, Miao D. BMI-1 mediates estrogen-deficiency-induced bone loss by inhibiting reactive oxygen species accumulation and T cell activation. J Bone Miner Res 2017;32:962–73.
[41] Siddiqi MZ, Siddiqi MH, Kim YJ, Jin Y, Huq MA, Yang DC. Effect of fermented red ginseng extract enriched in ginsenoside Rg3 on the differentiation and mineralization of preosteoblastic MC3T3-E1 cells. J Med Food 2015;18:542–8.
[42] Kim DY, Jung MS, Park YG, Yuan HD, Quan HY, Chung SH. Ginsenoside Rh2(S) induces the differentiation and mineralization of osteoblastic MC3T3-E1 cells through activation of PKD and p38 MAPK pathways. BMB Rep 2011;44:659–64.